ADVANCED MATERIALS
www.advmat.de

Tailoring Stress–Strain Curves of Flexible Snapping Mechanical Metamaterial for On-Demand Mechanical Responses via Data-Driven Inverse Design

*Zhiping Chai, Zisheng Zong, Haochen Yong, Xingxing Ke, Jiaqi Zhu, Han Ding, Chuan Fei Guo, and Zhigang Wu**

By incorporating soft materials into the architecture, flexible mechanical metamaterials enable promising applications, e.g., energy modulation, and shape morphing, with a well-controllable mechanical response, but suffer from spatial and temporal programmability towards higher-level mechanical intelligence. One feasible solution is to introduce snapping structures and then tune their responses by accurately tailoring the stress–strain curves. However, owing to the strongly coupled nonlinearity of structural deformation and material constitutive model, it is difficult to deduce their stress–strain curves using conventional ways. Here, a machine learning pipeline is trained with the finite element analysis data that considers those strongly coupled nonlinearities to accurately tailor the stress–strain curves of snapping metamaterialfor on-demand mechanical response with an accuracy of 97.41%, conforming well to experiment. Utilizing the established approach, the energy absorption efficiency of the snapping-metamaterial-based device can be tuned within the accessible range to realize different rebound heights of a falling ball, and soft actuators can be spatially and temporally programmed to achieve synchronous and sequential actuation with a single energy input. Purely relying on structure designs, the accurately tailored metamaterials increase the devices' tunability/programmability. Such an approach can potentially extend to similar nonlinear scenarios towards predictable or intelligent mechanical responses.

1. Introduction

Due to the introduction of delicately engineered building cells into the material, mechanical metamaterials exhibit unprecedented mechanical properties that those of natural materials are not comparable to, such as negative Poison's ratio,[1] negative compressibility,[2] high elastic stiffness,[3] and high strength-to-density ratio.[4] To enrich the functionality of mechanical metamaterials beyond these fixed mechanical properties, soft-material-based structures and connections can be introduced into the architecture.[5–9] These so-called flexible mechanical metamaterials exhibit excellent deformability and have endowed attractive applications concerned with structural deformation and transformation, such as adaptive surface conforming,[10] mechanical energy modulation,[11,12] and programmable shape morphing.[13–15] However, merely deformable structures are hard to be spatially and temporally programmed to form systems with highly precise and programmable mechanical responses toward high-level intelligence, such as mechanical signal transformation and computation,[16–19] reconfigurable mechanical properties,[20,21] and sequential behaviors.[22–24] One of the attractive solutions is to introduce snapping structures that can modulate the absorption and release of mechanical energy through their snap-through process.[25] By quantifying the relations between snapping structures and their corresponding mechanical responses, spatial and temporal behaviors of mechanical metamaterials can then be programmed for various specific applications that modulate mechanical signals. Quantifying the mechanical responses relies on an accurate depiction of the mechanical properties, and the most frequently adopted approach is to mathematically describe its stress–strain curve. As the stress–strain curve of structures contains abundant mechanical information, such as strain-dependent stiffness, required stress to achieve specific strain, and stored energy by deformed structures, the spatial and temporal mechanical responses can then be programmed on demand by tailoring the stress–strain curve.

Originating from the highly deformable and shape-transformable building cells, the behavior of snapping mechanical metamaterials is intrinsically nonlinear.[5] What is more, the complexity of such a nonlinear behavior increases with the introduction of more snapping structures, making it

Z. Chai, Z. Zong, H. Yong, X. Ke, J. Zhu, H. Ding, Z. Wu
State Key Laboratory of Intelligent Manufacturing Equipment and Technology
Huazhong University of Science and Technology
Wuhan 430074, China
E-mail: zgwu@hust.edu.cn
C. F. Guo
Department of Materials Science and Engineering
Southern University of Science and Technology
Shenzhen 518000, China

The ORCID identification number(s) for the author(s) of this article can be found under https://doi.org/10.1002/adma.202404369

DOI: 10.1002/adma.202404369

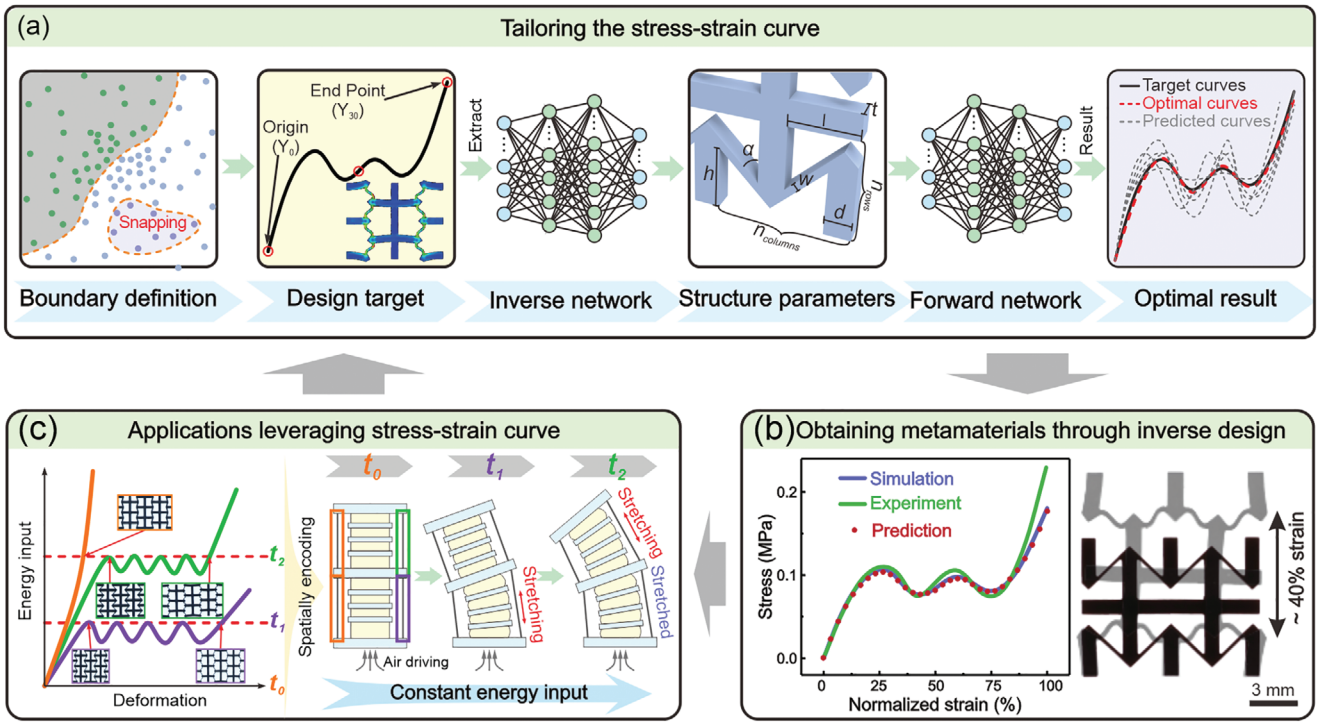

Figure 1. Tailoring the stress–strain curve of snapping mechanical metamaterials for on-demand mechanical responses via data-driven inverse design. a) Schematic of the FEA-based ML for the generation of snapping mechanical metamaterials with desired stress–strain curve. The overall ML pipeline consists of boundary determination, an inverse network, and a forward network. The boundary determination section describes the decision boundary of different mechanical response phases. The FEA results are extracted for training the neural networks. Eight structural parameters are determined to define the architecture of snapping mechanical metamaterials. b) Comparison of the stress–strain curves of the simulation, experiment, and predicted one. Taking a two-by-two snapping mechanical metamaterial with $w = 0.3$ mm, $l = 2.0$ mm, and $\alpha = 45°$ for example, the maximum nominal strain of the designed structure is around 40%. c) Demonstration of spatial and temporal motion programming with our approach.

harder to accurately depict the stress–strain curve with multiple snapping structures. Worse, due to the nonideal architecture and constraints (the structures that are hard to be simplified as hinges and beams, etc., of which boundary conditions are not fully constrained), composing soft materials with significant hyperelasticity, viscosity, and plasticity (such as polyurethanes and silicones) can sometimes undergo large and out-of-plane strain.[26–28] Therefore, highly nonlinear constitutive models of soft materials should also be seriously considered. Such strongly coupled nonlinear deformation and nonlinear constitutive model contribute to the difficulty of theoretically describing the stress–strain curve of snapping mechanical metamaterials.

Traditionally, a straightforward approach to describing the snapping behavior is to accurately derive the relations between the structural parameters and the corresponding mechanical responses by analytical modeling. Assuming linear elasticity and small local strain, various analytical models are deduced previously and widely adopted in investigating linear material constitutive model-based structures,[20,25,29] where nonlinear mechanical deformation can be accurately captured. However, it may encounter difficulties in analyzing large-strain structures with nonideal architecture and nonlinear constitutive models. Simplified spring models are thus utilized to understand the intrinsic physics of large-strain snapping structures,[30,31] while they suffer from the design accuracy of stress–strain curves. By fitting multilayer nonlinear mathematical mapping between the input and output data, machine learning (ML) is an emerging technique that is capable of tackling thorny coupling nonlinear problems in a computationally inexpensive way.[32] For instance, the tuning of stress–strain curves,[33,34] as well as other specific mechanical properties,[35–37] has been tried through ML-based methods recently. Moreover, instead of mapping the mathematical relation from structural parameters to mechanical properties, ML can also effectively map the relation from mechanical properties to structural parameters, which is the so-called inverse design. The ability to directly inverse design metamaterials from given mechanical properties accelerates the process of designing a structure for specific applications.[38] However, the aforementioned nonideal architecture, strongly coupled nonlinear mechanical deformation, and nonlinear constitutive models lead to the difficulty of obtaining enough high-quality datasets for further accurate ML training. That is, accurately tailoring the stress–strain curve of snapping mechanical metamaterials for on-demand mechanical responses remains challenging.

Combining the ML with finite element analysis (FEA) techniques, we propose an FEA-based ML method for accurately tailoring the stress–strain curve of flexible snapping mechanical metamaterial sheets (**Figure 1a**). In the beginning, strongly coupled nonlinear mechanical deformation and nonlinear constitutive models are considered in the FEA procedure to improve the quantification accuracy of the stress–strain curves. Then, an ML pipeline consisting of support vector machine (SVM)

classifiers, an inverse artificial neural network, and a forward artificial neural network is trained with the obtained FEA dataset and utilized to analyze the mechanical response phases and stress–strain curves. Consequently, the snapping metamaterial sheets with different types of mechanical responses can be inversely designed with an accuracy of 97.41% (a mean error of 2.59% in the testing dataset), and it is further verified by the FEA simulations and experiments (Figure 1b). Based on the established FEA-based ML approach, a data-driven inverse design framework comprising a three-step workflow to design snapping metamaterials is summarized as follows: first, based on the specific mechanical requirement from applications, the corresponding stress–strain curves are extracted (Figure 1c); second, according to these stress–strain curves, the ML pipeline inversely designs the structure of snapping metamaterial sheets; third, the designed snapping sheets are fabricated and demonstrated for their diverse applications. Finally, accurately tailored stress–strain curves for some typical applications are demonstrated, showing the potential of the proposed framework. For instance, the impact energy absorption efficiency of our snapping metamaterials can be tuned freely within its accessible range to adjust the rebound height of a falling ball, and different actuation modes of soft actuators can be spatially and temporally programmed to realize synchronous and sequential motion with a simple pneumatic input (Movie S1, Supporting Information).

2. Highly Nonlinear Behavior of Deformable Beam-Based Snapping Metamaterial

Based on a kind of thermoplastic polyurethane (TPU) material that is widely used in interactive intelligent systems,[22,39,40] we design a fully soft-beam-based snapping metamaterial sheet. From the perspective of mechanical behavior, TPU is also a representative nonlinear material featuring relatively significant hyperelasticity, viscosity, and plasticity (elaborated in Sections S1 and S2 in the Supporting Information). A successful design of TPU-based metamaterials lays the foundation for the design of other similar materials or those with simpler constitutive models, such as commonly used 3D printing material, polylactic acid (PLA), that can be regarded as linear elastic material, and widely adopted silicone polydimethylsiloxane (PDMS) that is typically coupled with hyperelasticity and viscosity.

Here, one type of the most widely adopted snapping structures[25] constrained beam elements, is leveraged to construct our snapping metamaterials. Due to the existence of multiple snapping behaviors during stretching, the stretchability of our designed snapping metamaterial sheets reaches up to 50%, which is far beyond the design range of state-of-the-art ML-based methods (refer to Section S10 in the Supporting Information).[32,34] The snapping building cell of our metamaterial consists of two symmetrically designed double-clamped tilt beams and three cantilever beams (as in Figure S1a in the Supporting Information). Once the upper end of the upper cantilever beam is displaced, the tilt beams are deformed and can sometimes induce snapping.[41] What is more, due to the co-existence of two cantilever beams on both sides of each unit cell, two ends of the tilt beam are not ideally clamped, making it even harder to predict the stress–strain curve of the cell-based metamaterials. Although other methods have been proposed to describe the behaviors of these nonideal chained beams,[42] their theories only work well under the premise that all the deformation and constitutive models are linear (Section S1, Supporting Information). Models for nonlinear constitutive materials still need to be studied, and thus we compared five types of analytical modeling and simulation methods of a single unit cell with experimental results (Figure S1d, Supporting Information). Thereby, it can be concluded that both geometric structure and highly nonlinear constitutive material contribute to the complexity of such a nontrivial model. Hence, it is reasonable to accurately test the constitutive model of the TPU material and analyze the force–displacement curve with FEA-based methods.

In our design, the mechanical metamaterial is constructed by an array of the aforementioned building cells. The architecture of metamaterials can thus be defined by eight structural parameters (the inset in Figure 1a), which are the number of columns (n_{columns}), the number of rows (n_{rows}), the height of a unit cell (h), the width of the cantilever beam (d), the horizontal length of the tilt beam (l), the angle between the cantilever beam and tilt beam (α), the width of the tilt beam (w), and the thickness of the metamaterial sheet (t). Among these structural parameters, h, d, and t are constants; n_{columns}, n_{rows}, l, α, and w have a more direct and predominant impact on the snapping behavior and are variables that can be tuned. In these tunable parameters, n_{columns} and n_{rows} are the array parameters that represent the size of metamaterials; l, α, and w are the geometry parameters that describe the geometric structure of each unit cell. Considering the influence of the moment of inertia, w^3 is also included in the geometry parameters (Section S4, Supporting Information).

During the investigation, we found that the phase of different mechanical responses is subjected to the structural parameters of metamaterials. In particular, both in-plane and out-of-plane deformations can occur under tension. When the metamaterial is under tension, the out-of-plane phase of mechanical responses will easily lead to interference with other objects in the system and hence cause undesired features in stress–strain curves (Figure S10, Supporting Information). Consequently, such out-of-plane behaviors make the corresponding response analysis/predictions very complex.[26] To avoid unnecessary phases of mechanical responses, the behavior of snapping metamaterials under tension is studied experimentally (**Figure 2a**; Figure S8a, Supporting Information). By varying the geometry parameters, the typical in-plane deformation and out-of-plane deformation can be observed. Furthermore, our tested data are classified by an SVM classifier, which divides the whole design space into two phases. As the decision boundary is apparently nonlinear, the radial basis function is used as our kernel function of SVM. The resulting SVM indicates that structures with large l, large w, and small α can cause out-of-plane deformation easily. Specifically, the in-plane and out-of-plane deformations are a combined effect of tilt beams and cantilever beams. With larger w and smaller α, the tilt beams tend to bend or twist out of the plane, where the required energy for its deformation is minimal. Similarly, with smaller l, the occurrence of the cantilever beam deformation is easier than the deformation of the tilt beam, which also leads to out-of-plane deformation. As in Figure 2b, the stress–strain curves of the in-plane deformation are smooth, whereas the out-of-plane stress–strain curves are

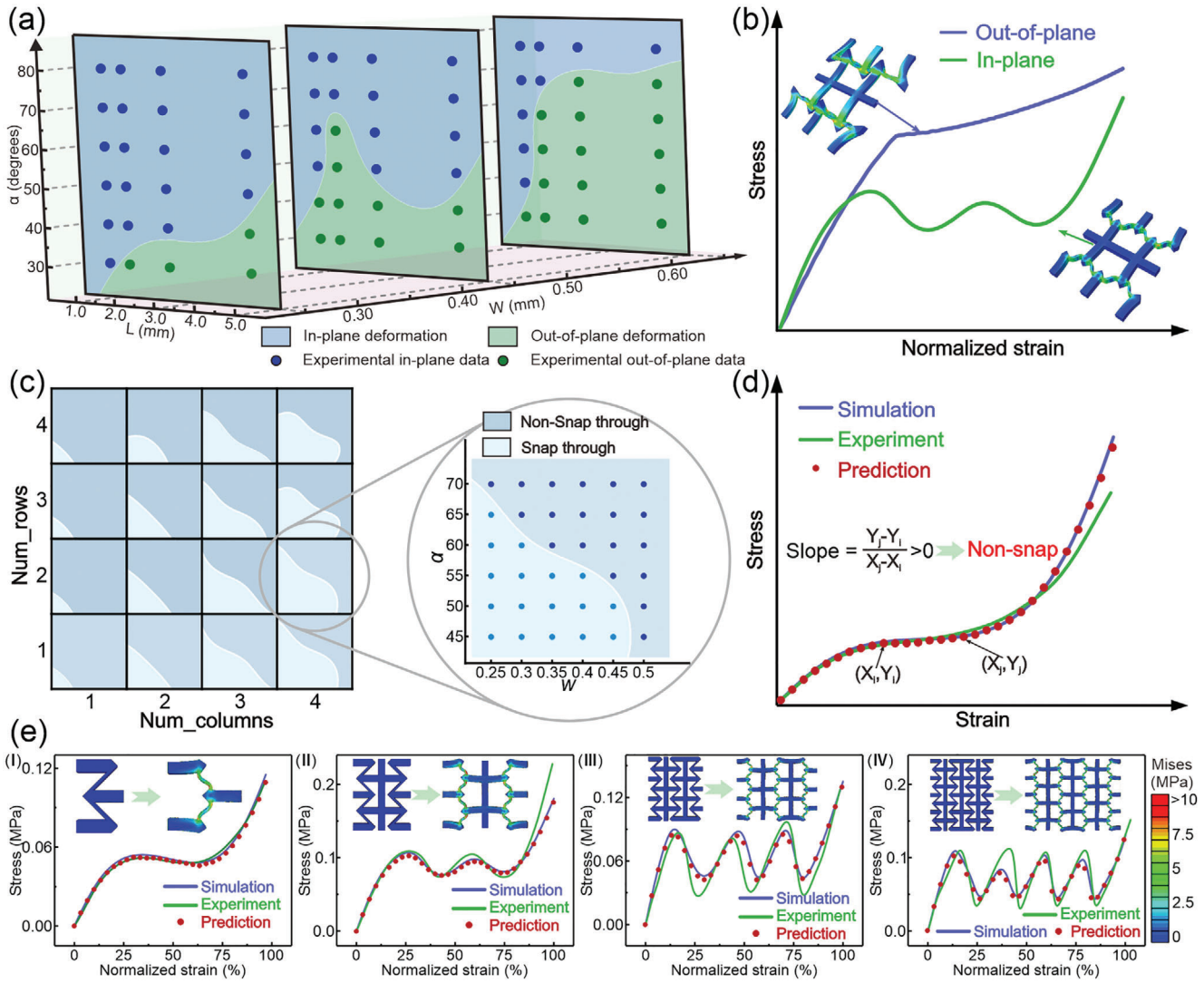

Figure 2. Decision boundary of different mechanical responses and the corresponding representative stress–strain curves. a) Decision boundary of the occurrence of the in-plane and out-of-plane deformations. b) The FEA result of the in-plane and out-of-plane deformations, and their corresponding stress–strain curves. c) Decision boundary of the occurrence of snapping and nonsnapping deformation. d) The simulation, experimental, and predicted stress–strain curves of nonsnap metamaterials. e) Four types of mechanical responses, in which snapping occurs, result in one wave, two waves, three waves, and four waves, respectively. The simulation, experimental, and predicted stress–strain curves of snapping metamaterials under tension are presented. The structural parameters of these metamaterials are provided in the Supporting Information.

usually featured by an abrupt turning point that represents an obvious out-of-plane deformation. In addition, the simulations including both the in-plane and out-of-plane phases match well with the experimental results (Figure S8b,c, Supporting Information).

Within the phase of in-plane deformation, the phases of nonsnapping and snapping are further studied. Given a certain value of l (l = 2.0 mm), the phase diagram of the snapping occurrence that is subjected to various structural parameters is plotted based on the simulation (Figure 2c). The SVM classifier is applied here again to determine the nonlinear decision boundary. It can be concluded that the larger the array size is, the easier the metamaterials are with identical geometry parameters snap. What is more, small α and w also result in the snapping behavior of the metamaterials. As in Figure 2d, typical stress–strain curves of the nonsnap metamaterials are monotonic and sometimes have an "S" shape with a plateau of a small slope. In contrast, those of the snapping metamaterials have negative slope regions (as in Figure 2e), and the number of which usually depends on the number of rows of building cells in the metamaterial. Generally, such a row-by-row snapping behavior from FEA agrees well with the experimental results, which implies the effectiveness of our FEA-based method in producing large amounts of data for ML. Notably, although the error between simulation and experimental results generally increases with the array size of the metamaterials, Figure 2d,e still shows the good accuracy of our FEA-based ML model within the phase of nonsnapping and snapping. When better computing resources are available, more precise

simulation methods may be developed in the future to further minimize the errors at local features (e.g., phase shift, peaks, and valleys), if necessary.

3. Detailed Architecture, Validation, and Optimization of the Neural Network

After the boundary determination by SVM classifiers, a snapping metamaterial sheet with target mechanical responses is then designed through a neural network. The neural network directly predicts the structural parameters of metamaterials with the desired stress–strain curves, facilitating a fast inverse design of snapping sheets. When collecting the data used for training the neural network, the metamaterials with the given geometry (w, w^3, l, and α) and array (n_{columns} and n_{rows}) parameters were calculated by FEA to obtain the corresponding force–displacement curves. Due to the inconsistency in each metamaterial's original lengths and total displacements, we normalized the data and transformed the force–displacement curves into the stress–strain curves (Section S6, Supporting Information). Then, a training dataset containing 2065 data samples is generated. Each set of the data consists of structural parameters $\boldsymbol{X}$ and corresponding stress–strain curve features $\boldsymbol{Y}$. Stress–strain curve features $\boldsymbol{Y}$ are the stress points extracted at uniform strain intervals from the FEA, and a total number of 31 stress points are extracted. With a cubic or spline interpolation method, a series of 31 points are accurate enough to reconstruct the original stress–strain curve, even for the curves with multiple peaks and valleys.

After the training dataset is obtained, a neural network can then be constructed for training. The neural network consists of an inverse network and a forward network, which are trained separately. To train the inverse network, stress–strain curve features $\boldsymbol{Y}$ and structural parameters $\boldsymbol{X}$ are the input and output (**Figure 3a**), respectively. For the forward network, the stress–strain curve features $\boldsymbol{Y}$ and structural parameters $\boldsymbol{X}$ are the output and input, respectively. Notably, due to the nonunique correspondence between stress–strain curve features $\boldsymbol{Y}$ and structural parameters X in the inverse design process, an inverse network is thus followed by a forward network to ensure that the output stress–strain curves match with the desired stress–strain curve features $\boldsymbol{Y}$ well.[33]

After proper data augmentation to complement our dataset (Section S6, Supporting Information), both networks are optimized using a randomized search followed by a finer grid search to determine the hyperparameters (Section S5, Supporting Information). An inverse neural network with 128 neurons in the first hidden layer and 600 neurons in the second hidden layer, and a forward neural network with 300 neurons in the first hidden layer and 800 neurons in the second hidden layer are finally determined. Due to the highly nonlinear behavior of metamaterials, a large network is essential, which contributes to a better fitting of the nonlinear stress–strain curves. The training epochs of the inverse neural network and forward neural network are finely tuned so that our model converges better and no obvious overfitting and underfitting occur (Section S5, Supporting Information). To improve the prediction accuracy, six inverse networks are connected parallelly to the identical forward network (more details in Section S5 in the Supporting Information). During a typical stress–strain curve design process, one optimal predicted curve and its corresponding structural parameters are selected among the six results. Then, to evaluate the predictive effectiveness of our model, a concept of relative error is introduced (Figure 3b). It is defined as the ratio of the area error divided by the area between the ground truth stress–strain curve and the normalized strain axis. The relative errors of each point in the training dataset and testing dataset (231 data samples that are never seen by the ML model) are calculated respectively. As in Figure 3c, by increasing the number of inverse networks in parallel, the prediction error of our ML model decreases by a ratio of about 50%. The individual relative error of each data point is plotted in Figure 3d,f, showing that most data points have good prediction accuracy. The mean relative errors of the training and testing dataset reach 1.08% and 2.59%, which implies accuracies of 98.92% and 97.41%, respectively. Moreover, the probability densities of relative errors for five types of mechanical responses (nonsnap, one wave, two waves, three waves, and four waves) are also analyzed. Based on Figure 3e,g, it can be concluded that our data augmentation method successfully balances the data amount of five types of mechanical responses, and nonsnap metamaterials tend to have smaller training-to-test result variation than metamaterials with snapping behaviors.

Notably, due to geometry conflict or the limitation of the adopted fabrication process, the selected optimal result of inverse design may generate structural parameters that are difficult to realize physically. Then all the results need to be checked to select the one that can be fabricated. Otherwise, the target stress–strain curve has to be compromised, and an alternative one that satisfies the requirement as well can be selected for inverse design.

4. Tunable Energy Absorption and Precisely Programmable Actuation Based on Snapping Metamaterials

Due to its unique fast-shifting behavior, snapping is widely harnessed in impact energy absorption,[43] programmable actuation,[24,25] and reconfiguration of soft actuators.[44] To demonstrate the capability of our design framework, a few metamaterials with the proposed snapping structure are fabricated for impact energy absorption and motion program.

The performance of energy absorption is often closely related to the energy changes during deformation. For snapping structures, the capability to absorb external energy depends on the local maximum and minimum values of the stress–strain curve and the stroke of the snap-through process.[20] To characterize the vibration-damping ability of the designed structure, we use the area of the snap-through process (product of stroke and fluctuation of the snap wave) to represent the absorbed energy (**Figure 4a**). Within our design range, the value range and boundary of the absorbed energy can then be identified (Figure 4b). Therefore, a suitable stress–strain curve and its corresponding metamaterial can be inversely designed to achieve a specific energy absorption efficiency as well as a target threshold force, which shows the ability of our inverse design method to co-design two mechanical properties. Specifically, a ball falls and hits the horizontally fixed metamaterials, and then the rebound heights are recorded to reflect the impact energy absorption efficiency of the snapping metamaterials, as in Figure 4c

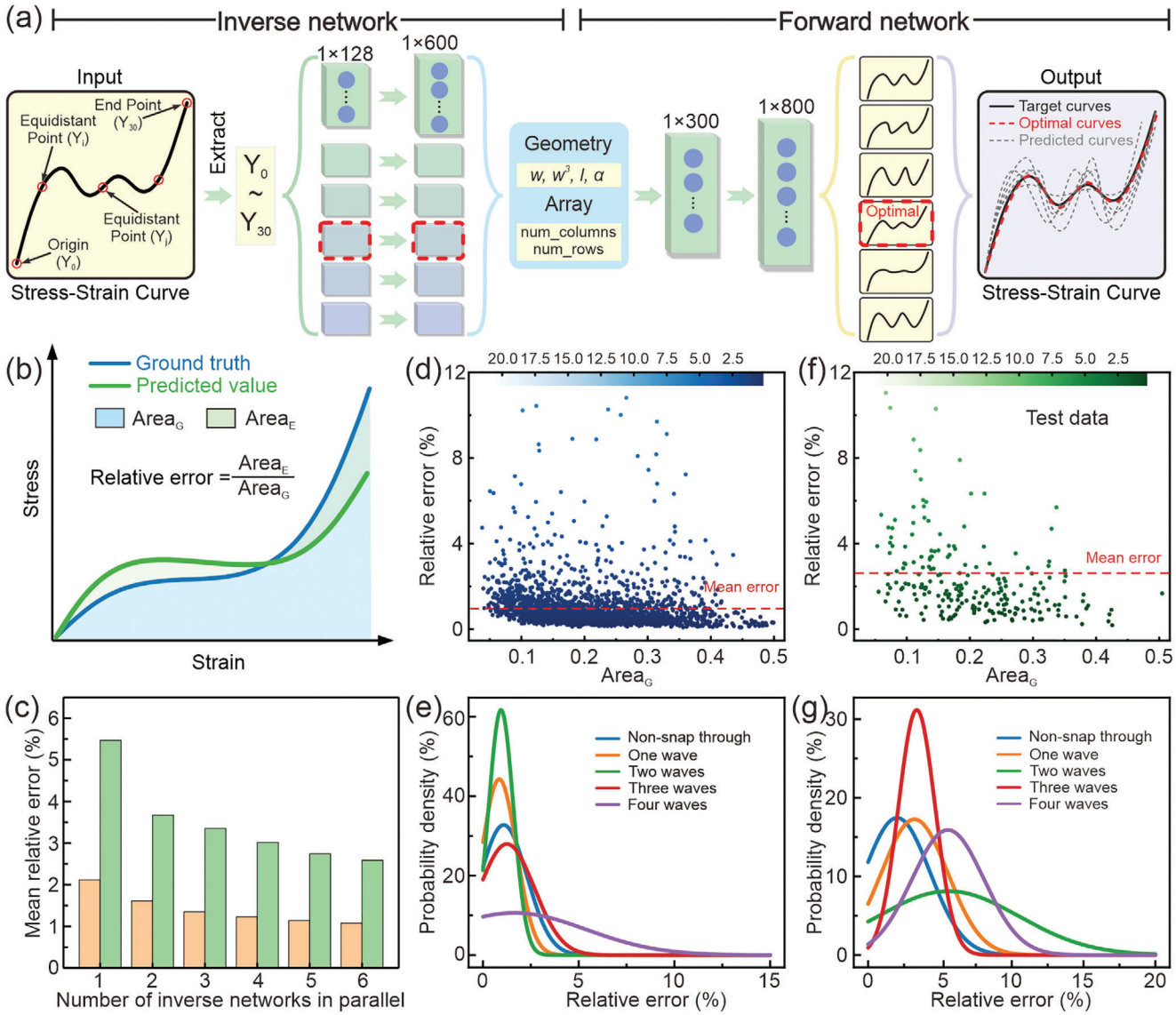

Figure 3. Evaluation and optimization of the neural network. a) The inverse network generates six sets of snapping mechanical metamaterials with different structural parameters that have stress–strain curves similar to that of the desired one. The forward network predicts the corresponding stress–strain curve of generated snapping mechanical metamaterials. b) Definition of the relative error. c) Change of mean relative error versus the number of inverse networks in parallel. d) The relative error points of training data (2065 samples) and f) testing data (231 samples). The probability density of relative error of five scenarios in the conditions of e) training data and g) testing data.

and in Movie S2 (Supporting Information). Then, three stress–strain curves with different energy absorption capabilities are selected and inversely designed to test the energy absorption efficiency (more details in Section S7 in the Supporting Information). Two of these metamaterials can snap under tension, and the other one is a typical nonsnap structure (Figure 4d–f). Both snapping metamaterials have identical snap-through thresholds but different energy absorption capabilities. The nonsnap metamaterial has an absorption efficiency of 86.0%. By contrast, the snapping metamaterials with different structural parameters have absorption efficiency values of 93.4% and 98.6%, respectively. Moreover, it is worth mentioning that the difference between the maximum and minimum rebound heights is tenfold, demonstrating a good tunability of absorption efficiency with our method.

As the behavior of soft actuators can be programmed by structural design,[45,46] our method can be further applied to improve the spatial and temporal behavior of reconfigurable soft actuators to increase their level of mechanical intelligence (**Figure 5**). By bolting different metamaterials on opposite sides of a pneumatic linear actuator (details in Section S8 in the Supporting Information), the soft actuators can realize three actuation modes, which are stretching, bending, and sequential bending under a simple pneumatic input. Hence, the actuation modes can be easily reconfigured by varying design parameters and replacing these metamaterial sheets. Since the output of soft actuators

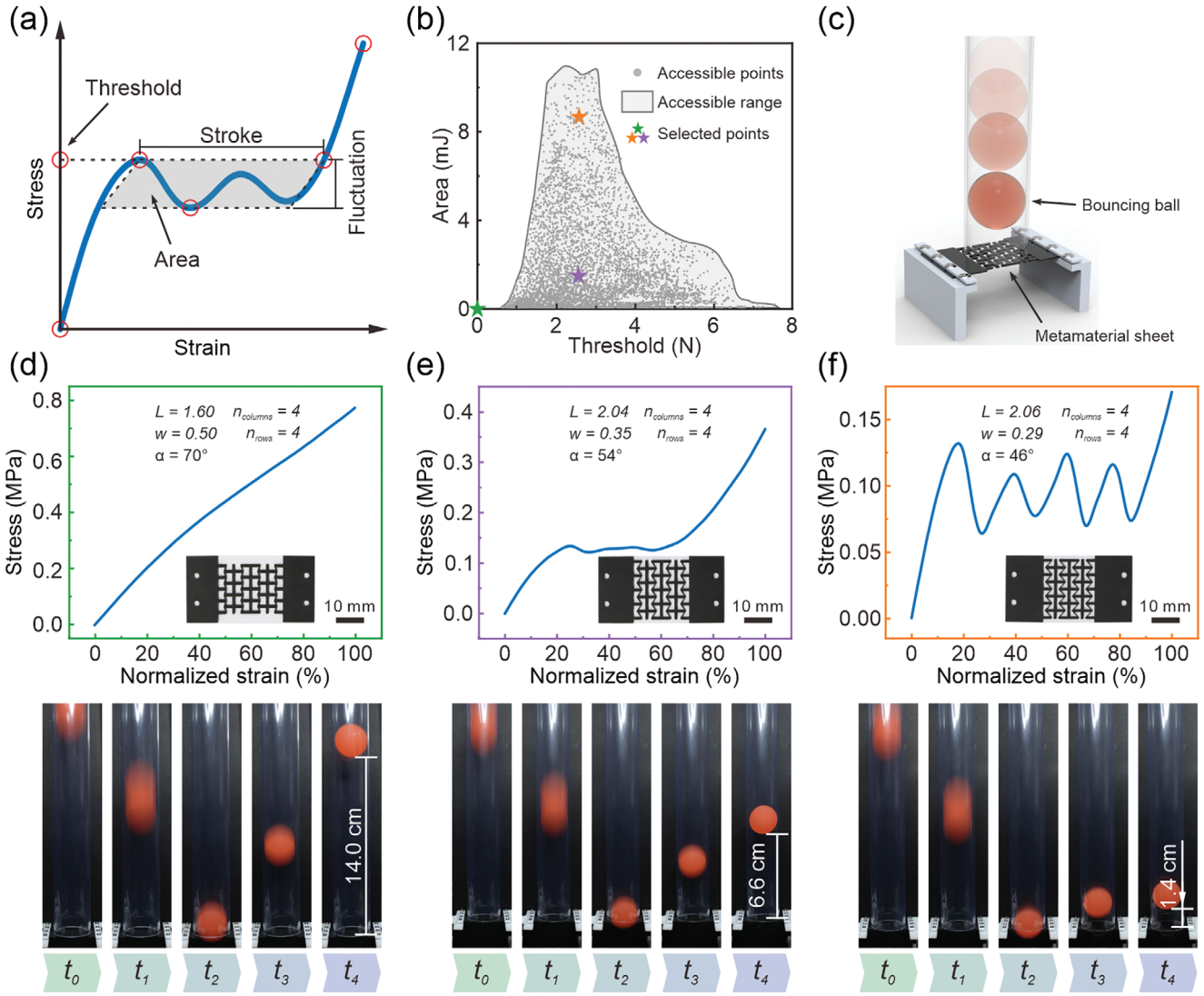

Figure 4. Tailoring the stress–strain curve of snapping mechanical metamaterials for tunable impact energy absorption. a) The energy absorbed by snapping metamaterials during impact is related to the area of the snap-through process. b) The accessible energy absorption range and the selected points that satisfy the corresponding threshold and energy absorption requirement. Two points with different thresholds but identical snap-through area are selected, and the other one has no threshold and snap-through area. c) The experimental setup of the impact energy absorption test. The snapping metamaterial sheet is fixed flat on the device to absorb the energy of a falling ball. The stress–strain curves and energy absorption ability of d) a non-snap metamaterial, e) a snapping metamaterial with a small snap-through area, and f) a snapping metamaterial with a large snap-through area.

is force, we convert the stress–strain curve that results from a displacement-controlled measurement to the strain–stress curve that results from a force-controlled measurement (Figure 5a). The waves in the stress–strain curve are flattened because the force exerted on the metamaterials becomes an independent variable, which originates from that the metamaterial will constantly deform once the applied tensile force reaches the snap-through threshold. Therefore, the deformation of snapping metamaterials before and after the snap-through process is regarded as small, making the spatial and temporal programmability of soft actuators possible. Achievable strain–stress curves within our inverse design range are then plotted, and four of them are inversely designed for target mechanical responses (Figure 5b; Figure S18, Supporting Information). These metamaterials are then bolted on opposite sides of a two-segment soft actuator to program its behavior (Figure 5c). Three of these metamaterials have a segment of strain–stress curve where the strain continuously rises with the stress kept constant. By contrast, the other one has a nonsnap structure, which is unable to realize snapping-induced large strain. As in Figure 5d,e and in Movie S3 (Supporting Information), the spatial and temporal programmability is determined by the stress–strain curve of these snapping metamaterials. When the snapping metamaterials with identical snap-through thresholds are bolted on opposite sides, the actuator elongates evenly. However, when the nonsnap metamaterials and snapping metamaterials are bolted on opposite sides of an actuator, the metamaterial with a snap-through threshold force mainly deforms, making the actuator bend toward the nonsnap

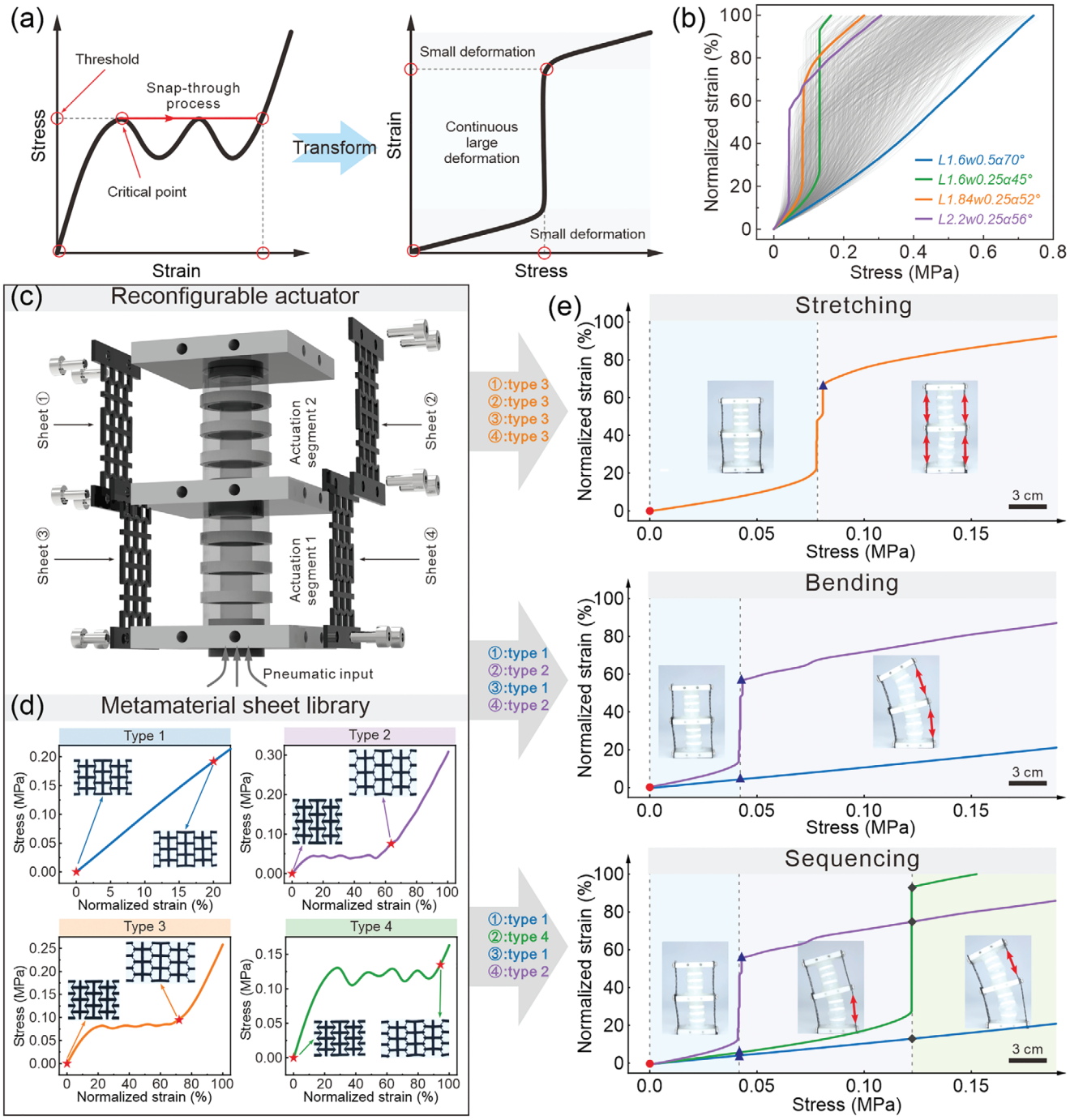

Figure 5. Tailoring the stress–strain curve of snapping mechanical metamaterials to spatially and temporally program a soft actuator. a) Stress–strain curve measured by a displacement-controlled method is transformed into a strain–stress curve measured by a force-controlled method. b) Possible range of predicted strain–stress curves and four generated curves for the programming of soft actuators. c) Detailed structure of the reconfigurable soft actuator based on our snapping metamaterials. The snapping metamaterials are bolted on the structure so that they can be easily reconfigured. d) Four snapping metamaterials and their corresponding strain–stress curves. The states of the fabricated metamaterial sheets before and after stretch are shown in the inset in the figure. e) Three actuation modes of the soft actuator are programmed by different combinations of snapping metamaterials, which are stretching, bending, and sequential bending. Different states of the actuation are labeled using different colors.

side. Then, the metamaterial with a snap-through threshold deforms until the applied stress exceeds the threshold value. Finally, leveraging the programmability of the actuation threshold, two metamaterials with different thresholds are integrated into the actuator together, and the actuator segment with a lower snap-through threshold deforms first. After the segment with a lower threshold finished bending, the strain within the actuator goes higher and the other segment of the actuator begins to bend. Therefore, an actuator with sequential motions can be configured on demand using our approach.

In addition, we further investigate the influence of strain rate on the behaviors of metamaterials. Due to the transition from rubber-like behavior to glassy-like behavior in high strain rates, the mechanical responses of the material are completely different,[47–49] making the stress–strain curves highly unpredictable. Hence, only the behavior of the TPU material under low strain rates is considered in this work. As elaborated in Section S2 (Supporting Information), higher strain rates lead to stiffer materials, which in turn increase the value of stress–strain curves of the metamaterials. However, the influences of strain rate on the metamaterials with different structural parameters are equivalent. As in Figure S5 (Supporting Information), with the strain rate changes, the relative relation between different stress–strain curves remains the same (for example, the curve of metamaterial-1 is always higher than that of metamaterial-2, and the curve of metamaterial-2 and metamaterial-3 always intersect with each other at the normalized strain of 0.7). Based on the above observations, we conducted some experiments where the soft actuators were driven under different actuation speeds. As in Figure S19 and Movie S4 (Supporting Information), the actuation of the soft actuator completed in 11, 5, and 2 s, respectively, and even the deformation sequence of each row of the cell unit in metamaterials remains identical. The result proves that different strain rates have little influence on the sequential motion of the soft actuator. Although extra simulations and experiments are needed to accurately predict the stress–strain curve under different strain rates, our inverse design framework is still viable, and the conclusion drawn under a specific strain rate will provide important information for the applications demonstrated under other strain rates.

In brief, the spatial and temporal programmability of snapping sheets mainly results from the snap-through process of the stress–strain curve. By extracting the specific mechanical characteristics, such as snap-through threshold, snap-through stroke, and snap-through related energy, needed for inverse design, a stress–strain curve that satisfies the requirement can be defined (Sections S7 and S8, Supporting Information). Then, following the three-step framework in Figure 1, snapping mechanical metamaterial sheets that facilitate truly mechanical intelligent applications can be fabricated on demand. Such an approach enables structurally encoded mechanical intelligence to simplify the constitution of the system and thus allows the actuator to achieve complex sequential behaviors for more tasks with simplified control.[50] Further, according to recent high-profile perspectives,[51,52] it can be envisioned that our three-step design framework can accelerate the accurate design of the next-generation flexible snapping structures for responsive and interactive systems with embodied mechanical intelligence.

5. Conclusion

Aiming to tackle the challenge of strongly coupled nonlinear deformation and constitutive model of soft snapping metamaterials, we propose a data-driven inverse design framework that can accurately tailor their stress–strain curves through an FEA-based ML approach to fulfill the target mechanical response demands of various applications. Owing to the high-quality data obtained from FEA and the good fitting capability of the neural networks, a decent accuracy has been achieved by our approach and further verified experimentally. Due to the strong adaptability of FEA and ML, our FEA-based ML thus provides a feasible framework that can be potentially adapted to the inverse design of other metamaterials with strongly coupled nonlinear deformation and constitutive models in the future.

6. Experimental Section

Sample Fabrication: First, the snapping pattern was drawn using commercial computer-aided software (AutoCAD 2021 and Autodesk Inventor 2022). Then, TPU sheets (from Alibaba, China) with a thickness of 0.8 mm were cut into the designed shapes via a UV laser marker system (GH-10U PRO, Huagong Laser, China). Finally, the cutting powder was removed from TPU surfaces using water or gas flushing. The calibration between the process and design parameters was obtained by a stereoscopic microscope (Stemi 508, Carl Zeiss, Germany).

Mechanical Testing: As in Figure S6 (Supporting Information), the hyperelasticity of TPU sheets was tested using a universal testing system (5944, Instron, USA), and the plasticity of TPU sheets was tested using a dynamic testing instrument (E1000, Instron, USA). The strain–stress curve of the designed snapping structures during the stretching process was recorded using a homemade test bench. The test bench (as in Figure S9 in the Supporting Information) was composed of a linear slide (from Alibaba, China), a force gauge (from Alibaba, China), and 3D-printed fixtures (PLA, Ultimaker S5, The Netherlands). The testing strain rate was consistent with the strain rate of material testing, which was 0.2 min^{-1}.

Finite Element Analysis-Based Simulations and Dataset Preparation: FEA simulations of the stress–strain curves of snapping structures were conducted using Abaqus 2023/explicit (Dassault Systèmes, France). The simulated samples were meshed in a C3D8R manner for dynamic analysis. The seeding of the overall sample was 0.2 relative size and 0.1 relative size for tilt beams. To maximally simulate the quasistatic behavior, the tension rate was set to be 0.4 mm s^{-1} (this tension rate in simulation was low enough for the quasistatic simulation of metamaterials; more details can refer to the Python script provided). The constitutive model of TPU material was fitted using the second-order polynomial model with user-fined plasticity (details in Sections S1 and S2 in the Supporting Information). To obtain enough simulation results for training the above neural network, a total of 2296 simulations were calculated by calling a script in Abaqus, among which 2065 samples were used for training and 231 samples were used for testing. A computer with two Intel Xeon Gold 5218R CPUs was used to obtain the simulation dataset, and it took around a month for the computer to compute. After the FEA calculation for each parameter, a txt file containing the strain–stress profile was generated. Then, MATLAB R2020b was used to postprocess these txt files and generate structural parameters X and stress–strain curve features Y accordingly. Specifically, the strain rates of the FEA simulation were the same with that of the experiments.

ML Model Setup and Evaluation: The inverse design neural network composed of an inverse network and a forward network was realized by multilayer perception networks in Python 3.9 (TensorFlow framework). The architecture optimization of neural networks was performed on a machine with NVIDIA GeForce GTX 1650 GPU, and all the optimization and training processes took about 6 days to complete. The structures of the two

networks were finally determined as 30 × 128 × 600 × 12 and 12 × 300 × 800 × 30, respectively. The input of the inverse network was the points on the stress–strain curve, and the output was structural parameters. For the forward network, the input and output were opposite. Before the training process, the input of the inverse model was augmented in an undifferentiated manner, but the input of the forward model was classified according to the shape of the stress–strain curve before augmentation. Detailed data processing procedure is elaborated in Supporting Information.

Demonstrations: The pipe in the ball rebound demonstration was made of polymethylmethacrylate (PMMA, from Alibaba, China). The bouncing height was recorded using a digital camera (EOS R5, Canon, Japan). The reconfigurable actuator was composed of 3D-printed stands (from Wenext, Shenzhen, China) and silicone air tubes (Ecoflex 00–30, Smooth-on, America). Adobe Premiere 2020 and ScreenToGif were used to extract photos and generate videos.

Statistical Analysis: The source dataset was obtained via FEA in Abaqus and divided into two parts (including in-plane metamaterials and out-of-plane metamaterials) using a trained SVM model. Then, due to the inconsistency in the original length and total displacement of each metamaterial, the data were normalized and the force–displacement curves were transformed into the stress–strain curves (see Section S6 in the Supporting Information). Due to the vibration of the quasistatic simulation, there could sometimes be fluctuation in the simulated stress–strain curve. The smooth function was used in MATLAB for smoothing all the stress–strain curves. Finally, the processed data were split into training (2065 samples) and testing (231 samples) datasets randomly. All steps above for statistical analysis were performed in Python.

Supporting Information

Supporting Information is available from the Wiley Online Library or from the author.

Acknowledgements

Z.C. and Z.Z. contributed equally to this work. This work was partially supported by the National Natural Science Foundation of China (Grant No. 52188102).

Conflict of Interest

The authors declare no conflict of interest.

Data Availability Statement

The data that support the findings of this study are openly available in snap-through at https://github.com/Zongzs123/snap-through, reference number 1.

Keywords

data-driven inverse design, mechanical metamaterial, programmable behavior, snapping, stress–strain curve

Received: March 26, 2024
Revised: June 6, 2024
Published online: June 28, 2024

[1] X. Ren, R. Das, P. Tran, T. D. Ngo, Y. M. Xie, *Smart Mater. Struct.* **2018**, *27*, 023001.
[2] Z. G. Nicolaou, A. E. Motter, *Nat. Mater.* **2012**, *11*, 608.
[3] J. B. Berger, H. N. G. Wadley, R. M. McMeeking, *Nature* **2017**, *543*, 533.
[4] J. Bauer, L. R. Meza, T. A. Schaedler, R. Schwaiger, X. Zheng, L. Valdevit, *Adv. Mater.* **2017**, *29*, 1701850.
[5] K. Bertoldi, V. Vitelli, J. Christensen, M. Van Hecke, *Nat. Rev. Mater.* **2017**, *2*, 17066.
[6] M. Mirkhalaf, A. Rafsanjani, *Matter* **2023**, *6*, 3719.
[7] X. Ke, H. Yong, F. Xu, H. Ding, Z. Wu, *Nat. Commun.* **2024**, *15*, 1491.
[8] A. Pala, M. Sitti, *Proc. Natl. Acad. Sci. USA* **2023**, *120*, 2212489120.
[9] L. A. Shaw, S. Chizari, M. Dotson, Y. Song, J. B. Hopkins, *Nat. Commun.* **2018**, *9*, 4594.
[10] S. Jiang, J. Liu, W. Xiong, Z. Yang, L. Yin, K. Li, Y. A. Huang, *Adv. Mater.* **2022**, *34*, 2204091.
[11] Q. Zeng, S. Duan, Z. Zhao, P. Wang, H. Lei, *Adv. Sci.* **2023**, *10*, 2204977.
[12] K. Barri, P. Jiao, Q. Zhang, J. Chen, Z. L. Wang, A. H. Alavi, *Nano Energy* **2021**, *86*, 106074.
[13] D. Wang, C. Jiang, G. Gu, *IEEE Trans. Robot.* **2023**, *40*, 606.
[14] X. Guo, W. Li, F. Fang, H. Chen, L. Zhao, X. Fang, Z. Yi, L. Shao, G. Meng, W. Zhang, *Sci. Adv.* **2024**, *10*, eadk3855.
[15] A. E. Forte, P. Z. Hanakata, L. Jin, E. Zari, A. Zareei, M. C. Fernandes, L. Sumner, J. Alvarez, K. Bertoldi, *Adv. Funct. Mater.* **2022**, *32*, 2111610.
[16] H. Zhang, J. Wu, D. Fang, Y. Zhang, *Sci. Adv.* **2021**, *7*, eabf1966.
[17] J. R. Raney, N. Nadkarni, C. Daraio, D. M. Kochmann, J. A. Lewis, K. Bertoldi, *Proc. Natl. Acad. Sci. USA* **2016**, *113*, 9722.
[18] W. Ye, L. Hu, H. Ou, T. Yu, *Sci. Adv.* **2023**, *9*, eadh3870.
[19] T. Mei, Z. Meng, K. Zhao, C. Q. Chen, *Nat. Commun.* **2021**, *12*, 7234.
[20] F. Pan, Y. Li, Z. Li, J. Yang, B. Liu, Y. Chen, *Adv. Mater.* **2019**, *31*, 1900548.
[21] Y. Yu, Y. Yin, R. Bai, Y. Hu, B. Li, M. Y. Wang, G. Chen, *Appl. Phys. Lett.* **2023**, *123*, 011702.
[22] T. R. Giri, R. Mailen, *Int. J. Mech. Sci.* **2021**, *204*, 106541.
[23] L. Jin, R. Khajehtourian, J. Mueller, A. Rafsanjani, V. Tournat, K. Bertoldi, D. M. Kochmann, *Proc. Natl. Acad. Sci. USA* **2020**, *117*, 2319.
[24] A. Rafsanjani, L. Jin, B. Deng, K. Bertoldi, *Proc. Natl. Acad. Sci. USA* **2019**, *116*, 8200.
[25] Y. Chi, Y. Li, Y. Zhao, Y. Hong, Y. Tang, J. Yin, *Adv. Mater.* **2022**, *34*, 2110384.
[26] Z. P. Wang, L. H. Poh, Y. Zhu, J. Dirrenberger, S. Forest, *Mater. Des.* **2019**, *170*, 107669.
[27] N. Hu, B. Li, R. Bai, K. Xie, G. Chen, *Research* **2023**, *6*, 0116.
[28] L. Jin, Y. Yang, B. O. T. Maldonado, S. D. Lee, N. Figueroa, R. J. Full, S. Yang, *Adv. Intell. Syst.* **2023**, *5*, 2300039.
[29] B. Haghpanah, L. Salari-Sharif, P. Pourrajab, J. Hopkins, L. Valdevit, *Adv. Mater.* **2016**, *28*, 7915.
[30] A. Rafsanjani, A. Akbarzadeh, D. Pasini, *Adv. Mater.* **2015**, *27*, 5931.
[31] M. Gomez, D. E. Moulton, D. Vella, *J. Mech. Phys. Solids* **2019**, *124*, 781.
[32] J. H. Bastek, D. M. Kochmann, *Nat. Mach. Intell.* **2023**, *5*, 1466.
[33] C. S. Ha, D. Yao, Z. Xu, C. Liu, H. Liu, D. Elkins, M. Kile, V. Deshpande, Z. Kong, M. Bauchy, X. R. Zheng, *Nat. Commun.* **2023**, *14*, 5765.
[34] B. Deng, A. Zareei, X. Ding, J. C. Weaver, C. H. Rycroft, K. Bertoldi, *Adv. Mater.* **2022**, *34*, 2206238.
[35] H. Pahlavani, M. Amani, M. C. Saldívar, J. Zhou, M. J. Mirzaali, A. A. Zadpoor, *Commun. Mater.* **2022**, *3*, 46.
[36] L. Zheng, S. Kumar, D. M. Kochmann, *Nat. Commun.* **2023**, *14*, 7563.
[37] J. Bastek, S. Kumar, B. Telgen, R. N. Glaesener, D. M. Kochmann, *Proc. Natl. Acad. Sci. USA* **2021**, *119*, 2111505119.
[38] X. Zheng, X. Zhang, T. Chen, I. Watanabe, *Adv. Mater.* **2023**, *35*, 2302530.
[39] A. A. Amiri Moghadam, S. Alaie, S. Deb Nath, M. Aghasizade Shaarbaf, J. K. Min, S. Dunham, B. Mosadegh, *Soft Robotics* **2018**, *5*, 443.

[40] C. Tawk, R. Mutlu, G. Alici, *Front. Robot. AI* **2022**, *8*, 799230.
[41] K. Che, M. Rouleau, J. Meaud, *Extrem. Mech. Lett.* **2019**, *32*, 100528.
[42] F. Ma, G. Chen, *Mech. Mach. Theor.* **2019**, *133*, 267.
[43] Z. Meng, Z. Ouyang, C. Q. Chen, *Compos. Struct.* **2021**, *271*, 114152.
[44] D. J. Preston, P. Rothemund, H. J. Jiang, M. P. Nemitz, J. Rawson, Z. Suo, G. M. Whitesides, *Proc. Natl. Acad. Sci. USA* **2019**, *116*, 7750.
[45] X. Ke, J. Jang, Z. Chai, H. Yong, J. Zhu, H. Chen, C. F. Guo, H. Ding, Z. Wu, *Soft Robotics* **2022**, *9*, 613.
[46] S. Zhang, X. Ke, Q. Jiang, Z. Chai, Z. Wu, H. Ding, *Adv. Mater.* **2022**, *34*, 2200671.
[47] J. Yi, M. C. Boyce, G. F. Lee, E. Balizer, *Polymer* **2006**, *47*, 319.
[48] H. Pouriayevali, Y. B. Guo, V. P. W. Shim, *Int. J. Impact Eng.* **2012**, *47*, 71.
[49] J. T. Fan, J. Weerheijm, L. J. Sluys, *Polymer* **2015**, *65*, 72.
[50] A. Rafsanjani, K. Bertoldi, A. R. Studart, *Sci. Rob.* **2019**, *7874*, eaav7874.
[51] P. Jiao, J. Mueller, J. R. Raney, X. R. Zheng, A. H. Alavi, *Nat. Commun.* **2023**, *14*, 6004.
[52] G. Mengaldo, F. Renda, S. L. Brunton, M. Bächer, M. Calisti, C. Duriez, G. S. Chirikjian, C. Laschi, *Nat. Rev. Phys.* **2022**, *4*, 595.